Author's Accepted Manuscript

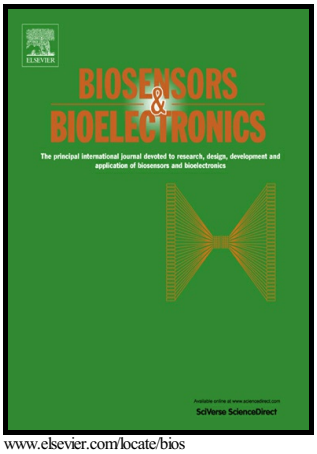

www.elsevier.com/locate/bios

Dual-reaction triggered sensitivity amplification for ultrasensitive peptide-cleavage based electrochemical detection of matrix metalloproteinase-7

Yun Zheng, Zhanfang Ma

PII: S0956-5663(18)30139-8
DOI: https://doi.org/10.1016/j.bios.2018.02.045
Reference: BIOS10307

To appear in: *Biosensors and Bioelectronic*

Received date: 23 November 2017
Revised date: 22 January 2018
Accepted date: 20 February 2018

Cite this article as: Yun Zheng and Zhanfang Ma, Dual-reaction triggered sensitivity amplification for ultrasensitive peptide-cleavage based electrochemical detection of matrix metalloproteinase-7, *Biosensors and Bioelectronic,* https://doi.org/10.1016/j.bios.2018.02.045

This is a PDF file of an unedited manuscript that has been accepted for publication. As a service to our customers we are providing this early version of the manuscript. The manuscript will undergo copyediting, typesetting, and review of the resulting galley proof before it is published in its final citable form. Please note that during the production process errors may be discovered which could affect the content, and all legal disclaimers that apply to the journal pertain.

ACCEPTED MANUSCRIPT

Dual-reaction triggered sensitivity amplification for ultrasensitive peptide-cleavage based electrochemical detection of matrix metalloproteinase-7

Yun Zheng, Zhanfang Ma*

Department of Chemistry, Capital Normal University, Beijing 100048, China

E-mail: mazhanfang@cnu.edu.cn

Accepted manuscript

ACCEPTED MANUSCRIPT

Abstract

In this work, a new strategy of dual-reaction triggered sensitivity amplification for ultrasensitive electrochemical detection of matrix metalloproteinase-7 (MMP-7) was developed. The sensitivity of amperometric biosensor relies on the current signal differences (ΔI) caused by per unit concentration target. Benefited from dual-reaction catalytic activities of Pd nanoparticles, dual catalytic reactions were implemented in the biosensor to amplify the ΔI: (1) Fenton-like reaction was triggered by the probes to degrade redox species methylene blue; (2) catalytic precipitation reaction was followed subsequently to generate insoluble precipitation by 4-chloro-1-naphthol oxidation. Dual-enhancement of ΔI triggered by Pd nanoparticle-based catalytic probes significantly improved the detection performance of the biosensor. The peptide-cleavage based biosensor integrated Pd nanoparticle-based catalytic probes with reduced graphene oxide-Au/methylene blue-sodium alginate hydrogel (Au-rGO/MB-SA) nanocomposites substrate for ultrasensitive detection of MMP-7. Under optimal conditions, the proposed biosensor exhibited a wide linear range from 10 fg mL^{-1} to 10 ng mL^{-1} with an ultralow detection limit of 3.1 fg mL^{-1}. This strategy successfully combines the multiple catalytic reactions triggered by nanomaterials with peptide-cleavage pattern in electrochemical biosensor, providing a promising method for detection of other proteases.

Keywords: matrix metalloproteinase-7, electrochemical biosensor, 4-chloro-1-naphthol, peptide cleavage, sodium alginate hydrogel

Accepted manuscript

ACCEPTED MANUSCRIPT

1. Introduction

Development method with simple catalytic materials for multiple-amplification of sensitivity is of great significance for efficient construction ultrasensitive electrochemical biosensors (Tang et al. 2017; Wang and Ma 2018; Wang et al. 2014). For amperometric immunosensors, the promotion of sensitivity depends on elevating the ΔI caused by per unit concentration target. Various strategies have been developed to enhance current signal via enrichment redox species (Cui et al. 2017; Kaushik et al. 2013), integration conductive materials (Cao et al. 2017; Hu et al. 2017; Yang et al. 2015) and employment catalytic reaction (Yang et al. 2018). To fully utilize the current signal, implementing multiple-triggered catalytic reactions based on simple and robust nanomaterials to further elevate the ΔI is an efficient approach (Yang et al. 2017).

MMP-7, a zinc and calcium dependent endopeptidase, is capable of degrading extracellular matrix (ECM) (Szarvas et al. 2010). According to reports, the MMP-7 level in healthy human serum ranged from 0.17 ng mL^{-1} to 3.5 ng mL^{-1} (Sarkissian et al. 2008). Increased expression of MMP-7 was correlated with the presence of metastatic disease and tumor differentiation. Ultrasensitive detection of MMP-7 is of significance for early cancer diagnosis and therapy. Compared to conventional immunoassay based on antibody-antigen recognition (Guo et al. 2011; Liu et al. 2015; Liu et al. 2012; Zayats et al. 2002; Zhao and Ma 2017), peptide cleavage mode applied in biomarker detection exhibits prominent advantages (Chen et al. 2013; Kou et al. 2017; Peng et al. 2016). For example, peptides are accessible and cost effectiveness, which can be obtained by phage display technique. In addition, shorter incubation time of peptides improves efficiency of sensing interface construction (Chalker et al. 2011; Orelma et al. 2012). Several nanomaterials have been applied for

Accepted manuscript

ACCEPTED MANUSCRIPT

sensitivity amplification in peptide cleavage-based electrochemical biosensor (Kou et al. 2016; Tang et al. 2016; Xu et al. 2016). As an important signal-transduction route, enzymatic biocatalytic reaction can form insoluble precipitation layer to improve the ΔI. Kou et al. (2016) and Tang et al. (2016) groups devised sensitivity amplified amperometric biosensor coupling with horseradish peroxidase or DNAzyme-based biocatalytic reaction. Despite the considerable advances in sensitivity, these approaches have some drawbacks: (1) easily denaturing with temperature and pH changes; (2) fussy labeling progress and complex modification. Enzyme-mimetic nanomaterials achieved simple synthesis and high chemical stability (Li et al. 2013; Wang et al. 2016). Benefited from their superior properties, some noble metal nanoparticles can trigger multiple reactions (Goodman et al. 2017; Ye et al. 2017). Particularly, Pd nanoparticles can react with hydrogen peroxide to produce reactive hydroxyl radicals (•OH), which are capable of degradation organic compound (Choudhary et al. 2007; Narayani et al. 2016; Tian et al. 2017; Voloshin et al. 2008; Yuan et al. 2011). In addition, as mimetic enzyme, Pd nanoparticles can catalyze 4-CN with H_2O_2 to generate insoluble precipitation (Das et al. 2009; Hou et al. 2014). If Fenton-like reaction and catalytic precipitation reaction based on Pd nanoparticles are introduced into amperometric biosensor, the detection performance of the biosensor will be substantially improved via amplifying the ΔI.

Herein, we proposed a dual-reaction triggered sensitivity amplification for ultrasensitive peptide-cleavage based electrochemical detection of MMP-7. Pd-polydopamine (Pd-PDA) nanocomposites were utilized as catalyst to trigger dual-reaction: (1) Fenton-like reaction was triggered by the probes to degrade redox species methylene blue (MB), elevating the current differences caused by target. (2) Catalytic precipitation reaction was followed subsequently to generate insoluble

Accepted manuscript

ACCEPTED MANUSCRIPT

precipitation by 4-CN oxidation, leading to further enhanced ΔI for sensitivity amplification. The peptide-cleavage based biosensor successfully integrated Pd nanoparticle-based catalytic probes with Au-rGO/MB-SA nanocomposites substrate for ultrasensitive detection of MMP-7. The proposed method has good performance in human serum sample analysis, suggesting the promising potential application in clinical analysis.

2. Experimental

2.1. Materials and Apparatus

$HAuCl_4 \cdot 3H_2O$, H_2PtCl_6, 4-CN, ascorbic acid (AA, 99.7%), dopamine hydrochloride (DA, 99%) and uric acid (UA) were purchased from Alfa Aesar (Tianjin, China). SA (alginic acid sodium salt from brown algea, low viscosity) and 11-mercaptoundecanoic acid ($HS(CH_2)_{11}COOH$) were purchased from Sigma-aldrich (Beijing, China). Trifluoroacetic acid (CF_3COOH) was obtained from J&K Scientific Ltd. (Beijing, China). Calcium chloride was bought from Beijing Chemical Reagents Company (Beijing, China). Graphene oxide (GO) was obtained from Nanjing JCNANO Tech Co. Ltd. (Nanjing, China). Methylene blue was obtained from Acros Organics (Beijing, China). Carcinoembryonic antigen (CEA) was purchased from Shanghai Linc-Bio Science Co. Ltd. (Shanghai, China). Bovine serum albumin (BSA, standard grade) was commercially obtained from Beijing Xinjingke Biotechnologies Co., Ltd. (Beijing, China). MMP-7 and matrix metalloproteinase-2 (MMP-2) were purchased from Sino Biological Inc. (Beijing, China). The peptide (NH_2-KKKRPLALWRSCCC-SH) was purchased from Science Peptide Biological Technology Co., Ltd. (Shanghai, China). Clinical human serum samples were provided by Deyi Diagnostics (Beijing, China). All solutions were prepared using deionized water. The phosphate buffer solution (PBS) contains 0.1 M NaCl and 10

Accepted manuscript

ACCEPTED MANUSCRIPT

mM phosphate buffer (pH 7.4).

Thermogravimetry was tested on NETZSCH STA 449F3 (NETZSCH, Germany). Scanning electron microscope (SEM) images were determined on HITACHI S-4800 SEM (HITACHI, Japan). Transmission electron microscope (TEM) images were determined on HITACHI H7650 TEM (HITACHI, Japan). Energy dispersive X-ray spectroscopy (EDS) was determined on HITACHI SU8010 SEM (HITACHI, Japan). Inductively coupled plasma mass-spectrometry (ICP-MS) was determined on Agilent 7500Ce (Agilent Technologies, America). All electrochemical measurements were carried out on CHI600 electrochemical workstation (Chenhua Instruments Co., Shanghai, China). Fourier transform infrared (FTIR) spectra were performed on a VECTORTM 22 spectrometer (Bruker, Germany). Ultraviolet-visible (UV-vis) spectroscopy measurements were performed on UV-3600 UV-vis spectrophotometer (Shimadzu, Japan). Zeta potential measurements were performed on Zetasizer Nano ZS (Malvern Instruments Co., UK). Ultrapure water used in all procedures was purified through Olst ultrapure K8 apparatus (Olst, Ltd., resistivity>18 MΩ). A three electrochemical system in experiment was composed of a glassy carbon electrode (GCE) (4 mm in diameter) as the working electrode, a platinum wire and an Ag/AgCl electrode as counter electrode and reference electrode, respectively.

2.2. Synthesis of Pd-SAM-PDA

Polydopamine (PDA) particles were prepared according to the previously literature (Ju et al. 2011). 40.5 mg dopamine hydrochloride was dissolved in 10 mL of deionized water. 380 μL of 0.5 mol/L NaOH solution was added to the dopamine hydrochloride solution at 50 °C. Under vigorous stirring for 5 h, PDA particles were centrifuged, washed by deionized water and retrieved as dispersed solution.

The self-assembled monolayer (SAM) of $HS(CH_2)_{11}COOH$ formed on the surface

Accepted manuscript

ACCEPTED MANUSCRIPT

of PDA particles was followed by the method reported previously (Wang et al. 2005). 0.2 mL CF_3COOH and 0.05 mL 100 mM $HS(CH_2)_{11}COOH$ dissolved in ethanol were added into PDA particles with stirring for 12 h. The obtained particles were retrieved by centrifugation and redispersed in 10 mL of deionized water.

For loading Pd nanoparticles, 120 μL 1% H_2PdCl_4 and 3 mL water were added into 2 mL SAM-PDA solution with stirring for 30 min. Then, to avoid the unspecific combination of MMP-7 and the active sites of Pd-SAM-PDA particles, 0.1% BSA solution was added to block the active sites with stirring for 1 h. BSA-Pd-SAM-PDA was centrifuged, thoroughly washed, diluted to 8.00 mL by deionized water and then stored at 4 °C. The concentration of Pd in BSA-Pd-SAM-PDA dispersed solution was 10.79 μg mL^{-1}, which was determined by ICP-MS.

2.3. Synthesis of Au-rGO

The preparation of Au-rGO was carried out by the citrate-mediated reduction of HAu_4Cl and GO. 4.00 mL 1.00 mg/L GO aqueous solution was added into 25.00 mL 0.05% HAu_4Cl solution with vigorous stirring for 2 h. 1.20 mL 0.20 M sodium citrate aqueous solution was added into the mixture with stirring for 1 h. Then the mixture was heated reflux for 1 h. After centrifugation (10000 rpm), Au-rGO was washed and redispersed in 8.00 mL deionized water.

2.4. Preparation of the biosensing platform

A glassy carbon electrode was polished with 0.05 μm alumina powders for 5 minutes and sonicated in ethanol and deionized water respectively. Then, 10 μL 0.2% SA aqueous solution, 20 μL 5mM $CaCl_2$ aqueous solution and 10 μL 10 mM MB aqueous solution were dropped on the surface of GCE step by step. After each step, the modified GCE was dried in 37 °C dryer. For removing the excessive MB on the surface of GCE, the electrode was washed by deionized water thoroughly. Then, 10

Accepted manuscript

ACCEPTED MANUSCRIPT

μL Au-rGO was dropped on the MB-SA hydrogel/GCE surface. 50 μL 50 μM peptide was incubated on the Au-rGO/MB-SA hydrogel/GCE for 1 h at 37°C. Then, 50 μL 0.10% glutaraldehyde was dropped on the surface of the modified electrode. After that, 50 μL BSA-Pd-SAM-PDA nanocomposites were incubated on the modified electrode for 1 h. After each modification operation, the modified electrode was washed by deionized water. To obtain the repeatability of the experimental results, all the concentration of MB solution, peptides solution and Pd in dispersed solution were consistent during electrodes modification process (optimization experiment of peptide concentration was not included).

2.5. Electrochemical measurement

80 μL 1 ng mL^{-1} MMP-7 was incubated on the BSA-Pd-SAM-PDA/peptides/Au-rGO/MB-SA hydrogel/GCE for 1 h. For catalytic degradation of MB, the obtained electrode was dipped in 100 mM H_2O_2 aqueous solution for 1 h. Then, for catalytic precipitation reaction, the electrode was dipped in 1.0 mM 4-CN solution containing 10 mM H_2O_2 for 30 min. Finally, the square wave voltammetry measurement was conducted from -0.5 to 0.2 V in 0.1 M phosphate buffered solution (pH=7.4) with pulse amplitude of 25 mV and an increase potential of 4 mV s^{-1}.

3. Results and discussion

3.1. Principle of the proposed peptide cleavage-based electrochemical sensor

Fabrication procedure and detection principle of the peptide cleavage-based electrochemical biosensor are demonstrated in Scheme 1. SA hydrogel with large specific surface was gelated on the surface of GCE. MB as redox species was absorbed into SA hydrogel mainly through electrostatic interaction. Au-rGO further improved the conductivity of sensing interface and it helped to immobilize peptides.

Accepted manuscript

ACCEPTED MANUSCRIPT

Pd-SAM -PDA nanocomposites were utilized as catalytic probes. BSA was used as blocking agent to avoid the unspecific combination of MMP-7 with active sites of Pd-SAM-PDA. Then, BSA-Pd-SAM-PDA nanocomposites were chemically linked with peptides by using glutaraldehyde. Target analyte MMP-7 specifically recognized and cleaved the peptides (NH2-KKKRPLALWRSCCC-SH). And it caused an indistinctive decrease in current signal by square wave voltammetry (SWV) measurement. Benefited from the superior catalytic activity of Pd-SAM-PDA nanocomposites, dual catalytic reactions were introduced in the biosensor to amplify ΔI: (1) redox species MB on the substrate was degraded via Fenton-like reaction triggered by Pd-based nanocomposites; (2) catalytic precipitation reaction was followed subsequently to generate precipitation with poor electrical conductivity by 4-CN oxidation. In this case, ultrasensitive detection of MMP-7 was successfully implemented in the biosensor.

Scheme 1

3.2. Characterization of MB-SA hydrogel and Au-rGO

The water content of SA hydrogel was measured to be 98.3% by thermogravimetry (Fig. S1). Zeta potentials of SA hydrogel and MB-SA nanocomposites were identified by Zetasizer Nano. The zeta potential of SA hydrogel was -80.8 mV (Fig. S2A). After SA hydrogel adsorbed MB, the zeta potential of MB-SA hydrogel changed to -41.5 mV (Fig. S2B). These results indicated that MB adsorption increased the zeta potential of the SA hydrogel and lowered surface charge.

The morphologies of Au-rGO, MB-SA hydrogel/GCE and Au-rGO/MB-SA hydrogel/GCE were characterized by TEM and SEM, respectively. Au nanoparticles were densely distributed on rGO sheets as shown in Fig. S3. The rough and porous surface structure of MB-SA hydrogel can be observed on the GCE (Fig. 1A). For

Accepted manuscript

ACCEPTED MANUSCRIPT

Au-rGO/MB-SA hydrogel, lamellar and folded structure loaded with Au nanoparticles appeared (Fig. 1B). The EDS showed the chemical compositions of MB-SA hydrogel and Au-rGO/MB-SA hydrogel. C, N, O, S and Ca were confirmed, which originated from MB-SA hydrogel (Fig. 1C). Compared with the MB-SA hydrogel, the Au-rGO/MB-SA hydrogel composites contained Au atom, indicating the successful modification of Au-rGO (Fig. 1D).

Fig. 1

3.3. Characterization of Pd-SAM-PDA

Surface chemistry of PDA particles was modulated by the formation of carboxylic acid-terminated alkanethiol monolayer. Pd nanoparticles were loaded on the surface of PDA particles. The PDA particles displayed homogeneous morphology and were about 250 nm in size (Fig. 2A). After immersion of PDA particles into an alkanethiol-containing solution ($HS(CH_2)_{11}COOH$ and CF_3COOH), a monolayer of carboxylic acid alkanethiol was formed on the corroded PDA surface through thiol-catechol/quinone adduct formation. As shown in Fig. 2B, the surface roughness of PDA particles was increased by the formation of carboxylic acid-terminated alkanethiol monolayer. For Pd-SAM-PDA particles, Pd nanoparticles were loaded on the edges of SAM-PDA particles (Fig. 2C). EDS showed the chemical compositions of PDA, SAM-PDA particles and Pd-SAM-PDA nanocomposites. C, N, O elements consisted in PDA particles (Fig. 2D). S element appeared (Fig. 2E) after the formation of carboxylic acid-terminated alkanethiol monolayer on PDA particles. Pd element was confirmed originated from Pd-SAM-PDA nanocoposites and the atomic ratio of Pd is 0.19% (Fig. 2F). To characterize the structural analysis of PDA, SAM-PDA particles and Pd-SAM-PDA nanocomposites, FTIR measurements were performed (Fig. S4). The two peaks at approximately 1603 and 1509 cm^{-1} of PDA particles were

Accepted manuscript

the characteristic peaks of indole and indoline structures (Nishizawa et al. 2016). The IR peaks at 1690 cm^{-1} for the SAM-PDA indicated the existence of the carboxylic acid functional groups, which further proved the successful grafting of carboxylic monolayer on PDA. In the spectrum of Pd-SAM-PDA, the peaks at approximately 638 and 500 cm^{-1} from the stretching vibrations of the Pd-O bonds indicated the interaction between Pd and carboxylic acids of SAM-PDA (Weng et al. 2014).

Fig. 2

3.4. Catalytic activities investigation of probes

To investigate the catalytic activity of BSA-Pd-SAM-PDA nanocomposites, UV-vis spectra were measured. As shown in Fig. S5, the aqueous solution of 10 μM MB gave an intense peak at 665 nm with a shoulder band at 625 nm (curve a). After the addition of 1 mM H_2O_2 into10 μM MB, the spectrum of the mixed solution was similar to that of pure MB solution (curve b). However, a decrease in maximum absorption of the mixed solution (4 mL 10 μM MB, 1 mM H_2O_2, 40 μL BSA-Pd-SAM-PDA dispersion) at 665 nm was observed, indicating that BSA-Pd-SAM-PDA nanocomposites had the catalytic potentials to degrade MB (curve c).

The degradation of MB dye solution through H_2O_2 using Pd loaded nanoparticles as catalysts occurs via the following Fenton-like reaction. H_2O_2 is decomposed on the surface of Pd^0 nanoclusters, Eq. (1) (Choudhary et al. 2007).

$$Pd^0 + 2H_2O_2 \rightarrow Pd^{2+} + 2{\bullet}OH + 2OH^- \quad (1)$$

$$C_{16}H_{18}N_3S^+ + 102{\bullet}OH \rightarrow 16CO_2 + 3NO_3^- + SO_4^{2-} + 6H^+ + 57H_2O \quad (2)$$

The •OH generated via chemical reaction presented in Eq. (1) subsequently attacks and decomposes the MB dye molecules, Eq. (2) (Baiju et al. 2007).

SEM analysis was taken to characterize the procedures of catalytic precipitation

Accepted manuscript

ACCEPTED MANUSCRIPT

reaction on the GCE. BSA-Pd-SAM-PDA nanocomposites were distributed on the surface of peptides/Au-rGO/MB-SA hydrogel/GCE (Fig. S6A). BSA-Pd-SAM-PDA nanocomposites were coated insoluble layer after the precipitation reaction, indicating that the insoluble benzo-4-chlorohexadienone was firmly fixed on the modified electrode (Fig. S6B).

3.5. Stepwise construction procedures of the biosensor

The stepwise construction procedures of the biosensor were measured by SWV, cyclic voltammetry (CV) and electrochemical impedance spectroscopy (EIS). As displayed in Fig. 3A and Fig. 3B, the current responses of MB-SA hydrogel modified GCE were shown (curve a) and enhanced by covering Au-rGO for large specific surface and excellent conductivity (curve b). The immobilization of peptides led to a significant decrease of signal current (curve c), due to the formation of electron-blocking layer. The current responses further declined after the peptides connected with Pd-SAM-PDA nanocomposites (curve d), suggesting that the conductivity of the modified electrode was decreased. After incubating MMP-7, the peak currents increased (curve e), indicating that the peptides were cleaved by MMP-7. Then, the current signals further decreased after catalytic degradation of MB (curve f) and precipitation reaction of 4-CN (curve g). EIS measurements were performed in 0.5 mM $[Fe(CN)_6]^{3-/4-}$ aqueous solution containing 0.1 M KCl. The semicircle diameter of the Nyquist plots corresponded to the electron transfer resistance (Fig. 3C). The bare glassy carbon electrode showed a small circle (curve a). After MB-SA hydrogel was coated on GCE, the diameter of semicircle increased (curve b). Then the peak current decreased by covering Au-rGO for its excellent conductivity (curve c), indicating that Au-rGO improved the conductivity of MB-SA hydrogel/GCE. The resistance increased when the peptides were immobilized on the

Accepted manuscript

substrate (curve d). After Pd-SAM-PDA nanocomposites were immobilized by using glutaraldehyde, the resistance decreased (curve e). When MMP-7 incubated on the substrate, the resistance slightly increased (curve f), indicating that peptides were cleaved by MMP-7. Finally, the resistance significantly increased after catalytic degradation of MB (curve g) and precipitation reaction of 4-CN (curve h).

Fig. 3

3.6. Optimization of detection conditions

As important factors for the detection performance of the biosensor, the quantity of peptides and the incubation time of peptides were optimized. The current signal gradually decreased with the increase of peptide concentration from 10 to 40 μM, the current signal kept constant from 40 to 50 μM (Fig. S7 A and B). To avoid nonspecific adsorption, 50 μM was chosen as the peptide concentration for biosensor. Then, the incubation time of peptide was optimized. The current signal of biosensor decreased gradually from 10 to 40 min, and it kept constant after 40 min (Fig. S8 A and B). Consequently, we chose 40 min as the incubation time.

The performance of dual-triggered reaction influenced the response sensitivity of the biosensor. Therefore, reaction time and H_2O_2 concentration of catalytic degradation reaction and catalytic precipitation reaction were optimized, respectively. When the catalytic degradation time of MB increased to 60 min, the electrochemical signal decreased and it kept constant from 60 to 100 min (Fig. S9 A and B). 60 min of catalytic degradation reaction was chosen for the subsequent experiments. And the current signal gradually decreased with the increase of H_2O_2 concentration from 10 to 100 mM. Then, the current signal remained constant when the concentration increased from 100 to 200 mM (Fig. S10 A and B). 100 mM H_2O_2 of the catalytic degradation reaction was chosen for the subsequent experiments. For the optimization of

Accepted manuscript

ACCEPTED MANUSCRIPT

precipitation reaction, when the precipitation reaction time increased to 40 min, the electrochemical signal decreased. With further increase of reaction time, the current signal remained constant (Fig. S11 A and B). 40 min of precipitation reaction time was used in experiments. As shown in Fig. S12 A and B, when the H_2O_2 concentration was less than 10 mM, with the increase of H_2O_2 concentration, the current signal decreased. Therefore, 10 mM H_2O_2 for precipitation reaction was chosen for the following detection analysis.

3.7. Signal amplification of dual-triggered reaction

The amplification effect of dual-reaction including degradation reaction of MB and catalytic precipitation reaction of 4-CN on the SWV responses was investigated under the optimal experimental conditions. To demonstrate the effect of peptide cleavage, the modified electrodes were incubated with and without 1 ng mL^{-1} MMP-7 and the SWV responses were recorded in Fig. 4A. The current difference ($\Delta I = I - I_0$, where I and I_0 are current peak of the biosensor incubated with and without 1 ng mL^{-1} MMP-7) was about 32.7 μA (Fig. 4A). To investigate the effect of Fenton-like reaction, the modified electrodes were subsequently dipped in 100 mM H_2O_2 aqueous solution for 1 h to perform Fenton-like reaction after the electrodes were incubated with and without 1 ng mL^{-1} MMP-7. The SWV current difference was enlarged to 110.5 μA (Fig. 4B). To confirm the effect of catalytic precipitation reaction, 4-CN oxidation reaction and MB degradation reaction were implemented in the modified electrodes after the electrodes were incubated with and without 1 ng mL^{-1} MMP-7. The SWV current difference was further increased to 189.4 μA (Fig. 4C). These results further indicated that dual-triggered reaction can significantly increase ΔI caused by per unit concentration MMP-7 to promote detection performance of the biosensor.

Fig. 4

Accepted manuscript

ACCEPTED MANUSCRIPT

3.8. Performance of proposed biosensor

The SWV responses for different concentrations of MMP-7 were performed under optimized conditions. As shown in Fig. 5, the current signal decreased with decreasing concentration of MMP-7. The calibration plot showed a promising relationship between the current signal and MMP-7 concentration, ranging from 0.01 pg mL^{-1} to 10 ng mL^{-1}. The linear equation is $\Delta I=29.93 \log_{10}C_{MMP-7}+190.39$, where R^2 is 0.9987. The ultralow detection limit of the biosensor is 3.1 fg mL^{-1} for MMP-7 at a signal-to-noise ratio of 3σ (S/N=3) (σ is the standard deviation of signal in a blank solution). Compared with recently published literatures of detection MMP-7 based on peptide-cleavage, the biosensor exhibits lower detection limit (Table S1).

Fig.5

3.9. Evaluation of repeatability, specificity and stability of the biosensor

MMP-2, UA, AA, CEA and BSA were used as distractions to analyze the selectivity of this biosensor. When the biosensor was incubated with MMP-2 (100 ng mL^{-1}), UA (30 μg mL^{-1}), AA (10 μg mL^{-1}), CEA (100 ng mL^{-1}) and BSA (100 ng mL^{-1}), respectively, the current response changes are negligible compared with that of the biosensor incubated with 1 ng mL^{-1} MMP-7. When MMP-7 was coexisted with the proposed distractions, the current signal vibrations were almost the same as that with only MMP-7 (Fig. S13). These results indicated that the biosensor exhibited good specificity for MMP-7. The repeatability was analyzed using five modified electrodes, incubated with 0.001, 0.01, 0.1, 1 and 10 ng mL^{-1} MMP-7, respectively, and the corresponding standard deviations were 2.7%, 1.9%, 4.8%, 4.6%, and 1.4%, respectively, indicating that good repeatability of the biosensor. To investigate the stability of the biosensor, the biosensor was stored at 4 °C for 30 days and the electrochemical performance of the biosensor for MMP-7 was evaluated. The

Accepted manuscript

ACCEPTED MANUSCRIPT

electrochemical signal showed approximate value with the RSD of less than 10%, indicating that remarkable stability of the biosensor.

3.10. Practical application of the biosensor

Recovery experiments were carried out by adding five various concentrations of MMP-7 into healthy human serum. As shown in Table S2, the recoveries ranged from 96.3% to 104%, suggesting the promising reliability application in clinical analysis.

4. Conclusion

In summary, an ultrasensitive biosensor was successfully developed for detection of MMP-7 based on dual-reaction triggered sensitivity amplification. The multi-functional probes Pd-SAM-PDA nanocomposites achieved remarkable catalytic activity and simple synthesis. Fenton-like reaction and catalytic precipitation reaction triggered by nanoprobes significantly enlarged ΔI for sensitivity amplification. The smart biosensor based on peptide-cleavage successfully combined with dual catalytic reactions and exhibited ultralow detection limit of MMP-7. Present strategy based on peptide-cleavage can be easily extended to the detection of other proteases.

Acknowledgements

This research was financed by grants from the National Natural Science Foundation of China (21273153, 21673143), Natural Science Foundation of Beijing Municipality (2172016, 2132008), and the Project of the Construction of Scientific Research Base by the Beijing Municipal Education Commission.

References

Baiju, K.V., Shukla, S., Sandhya, K.S., J. James, A., Warrier, K.G.K., 2007. J. Phys. Chem. C 111, 7612-7622.

Cao, J.T., Yang, J.J., Zhao, L.Z., Wang, Y.L., Hui, W., Liu, Y.M., Ma, S.H., 2017. Biosens. Bioelectron. 99, 92-98.

Accepted manuscript

ACCEPTED MANUSCRIPT

Chalker, J.M., Bernardes, G.J., Davis, B.G., 2011. Acc. Chem. Res. 44, 730-741.

Chen, P., Selegård, R., Aili, D., Liedberg, B., 2013. Nanoscale 5, 8973-8976.

Choudhary, V.R., Samanta, C., Jana, P., 2007. Appl. Catal. A-Gen. 332, 70-78.

Cui, L., Li, Y.Y., Lu, M.F., Tang, B., Zhang, C.Y., 2017. Biosens. Bioelectron. 99, 1-7.

Das, J., Kim, H., Jo, K., Park, K.H., Jon, S., Lee, K., Yang, H., 2009. Chem. Commun. , 6394-6396.

Goodman, E.D., Dai, S., Yang, A.C., Wrasman, C.J., Gallo, A., Bare, S.R., Hoffman, A.S., Jaramillo, T.F., Graham, G.W., Pan, X., 2017. ACS Catal. 7, 4372-4380

Guo, S.J., Wen, D., Zhai, Y.M., Dong, S.J., Wang, E.K., 2011. Biosens. Bioelectron. 26, 3475-3481.

Hou, L., Gao, Z.Q., Xu, M.D., Cao, X., Wu, X.P., Chen, G.N., Tang, D.P., 2014. Biosens. Bioelectron. 54, 365-371.

Hu, Y.F., Zhang, Q.Q., Guo, Z.Y., Wang, S., Du, C.N., Zhai, C.Y., 2017. Biosens. Bioelectron. 98, 91-99.

Ju, K.Y., Lee, Y., Lee, S., Park, S.B., Lee, J.K., 2011. Biomacromolecules 12, 625-632.

Kaushik, A., Vasudev, A., Arya, S.K., Bhansali, S., 2013. Biosens. Bioelectron. 50, 35-41.

Kou, B.B., Chai, Y.Q., Yuan, Y.L., Yuan, R., 2017. Anal. Chem. 89, 9383-9387.

Kou, B.B., Zhang, L., Xie, H., Wang, D., Yuan, Y.L., Chai, Y.Q., Yuan, R., 2016. ACS Appl. Mater. Interfaces 8, 22869-22874.

Li, J.S., Jia, Y.H., Zheng, J., Zhong, W.W., Shen, G.L., Yang, R.H., Tan, W.H., 2013. Chem. Commun. 49, 6137-6139.

Liu, J.Y., Wang, J., Wang, T.S., Li, D., Xi, F.N., Wang, J., Wang, E.K., 2015. Biosens. Bioelectron. 65, 281-286.

Accepted manuscript

ACCEPTED MANUSCRIPT

Liu, Y., Liu, Y., Feng, H.B., Wu, Y.M., Joshi, L., Zeng, X.Q., Li, J.H., 2012. Biosens. Bioelectron. 35, 63-68.

Narayani, H., Augustine, R., Sumi, S., Jose, M., Nair, K.D., Samsuddin, M., Prakash, H., Shukla, S., 2016. Sep. Purif. Technol. 172, 338-349.

Nishizawa, N., Kawamura, A., Kohri, M., Nakamura, Y., Fujii, S., 2016. Polymers 8, 62.

Orelma, H., Teerinen, T., Johansson, L.S., Holappa, S., Laine, J., Biomacromolecules 2012. 13, 1051-1058.

Peng, K.F., Zhao, H.W., Xie, P., Hu, S., Yuan, Y.L., Yuan, R., Wu, X.F., Biosens. Bioelectron. 2016. 81, 1-7.

Sarkissian, G., Fergelot, P., Lamy, P.J., Patard, J.J., Culine, S., Jouin, P., Rioux-Leclercq, N., Darbouret, B., 2008. Clin. Chem., 54, 574-581.

Szarvas, T., Becker, M., Vom, D.F., Gethmann, C., Tötsch, M., Bánkfalvi, A., Schmid, K.W., Romics, I., Rübben, H., Ergün, S., 2010. Cancer Science, 101, 1300-1308.

Tang, Z.X., Fu, Y.Y., Ma, Z.F., 2017. Biosens. Bioelectron. 91, 299-305.

Tang, Z.X., Wang, L.Y., Ma, Z.F., 2017. Biosens. Bioelectron. 92, 577-582.

Tian, P.F., Ouyang, L.K., Xu, X.Y., Ao, C., Xu, X.C., Si, R., Shen, X.J., Lin, M., Xu, J., Han, Y.F., 2017. J. Catal. 349, 30-40.

Voloshin, Y., Manganaro, J., Lawal, A., 2008. Ind. Eng. Chem. Res. 47, 8119-8125.

Wang, H., Chen, S.F., Li, L.Y., Jiang, S.Y., 2005. Langmuir 21, 2633-2636.

Wang, H.Q., Ma, Z.F., 2018. Sensor. Actuat. B: Chem. 254, 642-647.

Wang, L.D., Liu, Y., Li, J.H., 2014. Anal. Chem. 86, 7907-7912.

Wang, Q.Q., Zhang, L.L., Shang, C.S., Zhang, Z.Q., Dong, S.J., 2016. Chem. Commun. 52, 5410-5413.

Weng, X., Ren, H., Chen, M., Wan, H., 2014. ACS Catal. 4, 2598-2604.

Accepted manuscript

ACCEPTED MANUSCRIPT

Xu, W.J., Jing, P., Yi, H.Y., Xue, S.Y., Yuan, R., 2016. Sensor. Actuat. B: Chem. 230, 345-352.

Yang, G.H., Zhu, C.Z., Du, D., Zhu, J.J., Lin, Y.H., 2015. Nanoscale 7, 14217-14231.

Yang, W.Q., Huang, T.T., Zhao, M.M., Luo, F., Weng, W., Wei, Q.H., Lin, Z.Y., Chen, G.N., 2017. Talanta 164, 1-6.

Yang, Y.Y., Yan, Q., Liu, Q., Li, Y.P., Liu, H., Wang, P., Chen, L., Zhang, D.P., Li, Y.Y., Dong, Y.H., 2018. Biosens. Bioelectron. 99, 450-457.

Ye, T., Durkin, D.P., Banek, N.A., Wagner, M.J., Shuai, D.M., 2017. ACS Appl. Mater. Interfaces 9, 27421-27426.

Yuan, S.H., Fan, Y., Zhang, Y.C., Tong, M., Liao, P., 2011. Environ. Sci. Technol. 45, 8514-8520.

Zayats, M., Raitman, O.A., Chegel, V.I., Kharitonov, A.B., Willner, I., 2002. Anal. Chem. 74, 4763-4773.

Zhao, L.H., Ma, Z.F., 2017. Sensor. Actuat. B: Chem. 241, 849-854.

Accepted manuscript

ACCEPTED MANUSCRIPT

Figure Captions

Scheme 1. Schematic illustrations of the dual-reaction triggered sensitivity amplification for peptide-cleavage based electrochemical biosensor.

Fig. 1. Characterization of Au-rGO/MB-SA hydrogel composites substrate. SEM images of MB-SA hydrogel/GCE (inset: magnified one) (A), Au-rGO/MB-SA hydrogel/GCE (inset: magnified one) (B). EDS of MB-SA hydrogel (C), and Au-rGO/MB-SA hydrogel composites (D).

Fig. 2. Characterization of Pd-SAM-PDA nanocomposites. SEM images of PDA particles (A), SAM-PDA particles (B), Pd-SAM-PDA nanocomposites (C). EDS of PDA (D), SAM-PDA (E), Pd-SAM-PDA nanocomposites (F).

Fig. 3. SWV (A) and CV (B) of different modified electrodes in 0.1 M phosphate buffered solution (pH=7.4): MB-SA hydrogel/GCE (a), Au-rGO/MB-SA hydrogel/GCE (b), peptides/Au-rGO/MB-SA hydrogel/GCE (c), BSA-Pd-SAM-PDA/peptides/Au-rGO/MB-SA hydrogel/GCE (d), incubated with MMP-7 (e), treated by catalytic degradation reaction of MB (f), treated by catalytic precipitation reaction (g). Nyquist plots of different modified electrodes in 0.1 M phosphate buffered solution (pH=7.4) (C): bare electrode (a), MB-SA hydrogel/GCE (b), Au-rGO/MB-SA hydrogel/GCE (c), peptides/Au-rGO/MB-SA hydrogel/GCE (d), BSA-Pd-SAM-PDA/peptides/Au-rGO/MB-SA hydrogel/GCE (e), incubated with MMP-7 (f), treated by catalytic degradation reaction of MB (g), treated by catalytic precipitation reaction (h). Inset: Magnified view of Nyquist plots of bare electrode (a), MB-SA hydrogel/GCE (b), Au-rGO/MB-SA hydrogel/GCE (c), peptides/Au-rGO/MB-SA hydrogel/GCE (d).

Fig. 4. The comparison of SWV current signal differences: the biosensor without dual-reaction amplification (A), the biosensor only treated with catalytic degradation

Accepted manuscript

ACCEPTED MANUSCRIPT

reaction of MB (100 mM H_2O_2 for Fenton-like reaction) (B) and the biosensor treated with dual-reaction amplification (100 mM H_2O_2 for Fenton-like reaction, 10 mM H_2O_2 and 1.0 mM 4-CN for catlytic precipitation reaction) (C). The biosensor was incubated with 1 ng mL^{-1} MMP-7 (red lines) and with 0 ng mL^{-1} MMP-7 (black lines) (in 0.1 M phosphate buffered solution, pH=7.4).

Fig. 5. (A) SWV responses of electrochemical detection for MMP-7 in 0.1 M phosphate buffered solution (pH=7.4) at the concentrations from 10 fg mL^{-1} to 10 ng mL^{-1}. (B) The calibration plot between the SWV peak current (-0.145 V vs. Ag/AgCl) and the logarithm values of MMP-7 concentrations (the error bars are standard deviations for n=3).

Highlights

1. New type peptide-cleavage based amperometric biosensor was developed.
2. Pd-polydopamine based probe triggered dual-reaction for sensitivity amplification.
3. The biosensor showed linear range from 10 fg mL^{-1} to 10 ng mL^{-1} with detection limit of 3.1 fg mL^{-1}.

Accepted manuscript

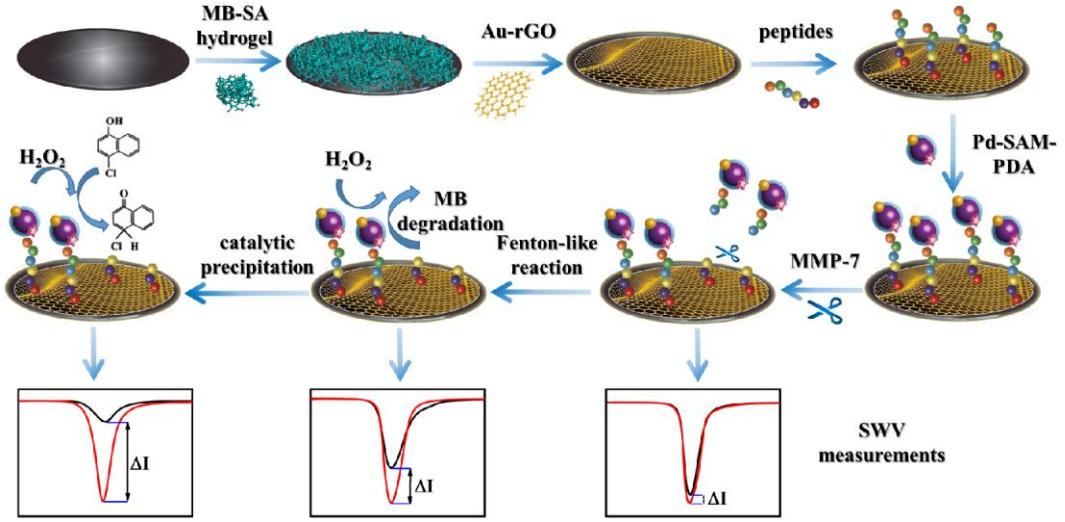
MB-SA hydrogel
Au-rGO
peptides
Pd-SAM-PDA
MMP-7
Fenton-like reaction
MB degradation
catalytic precipitation
H_2O_2
H_2O_2
ΔI
ΔI
ΔI
SWV measurements

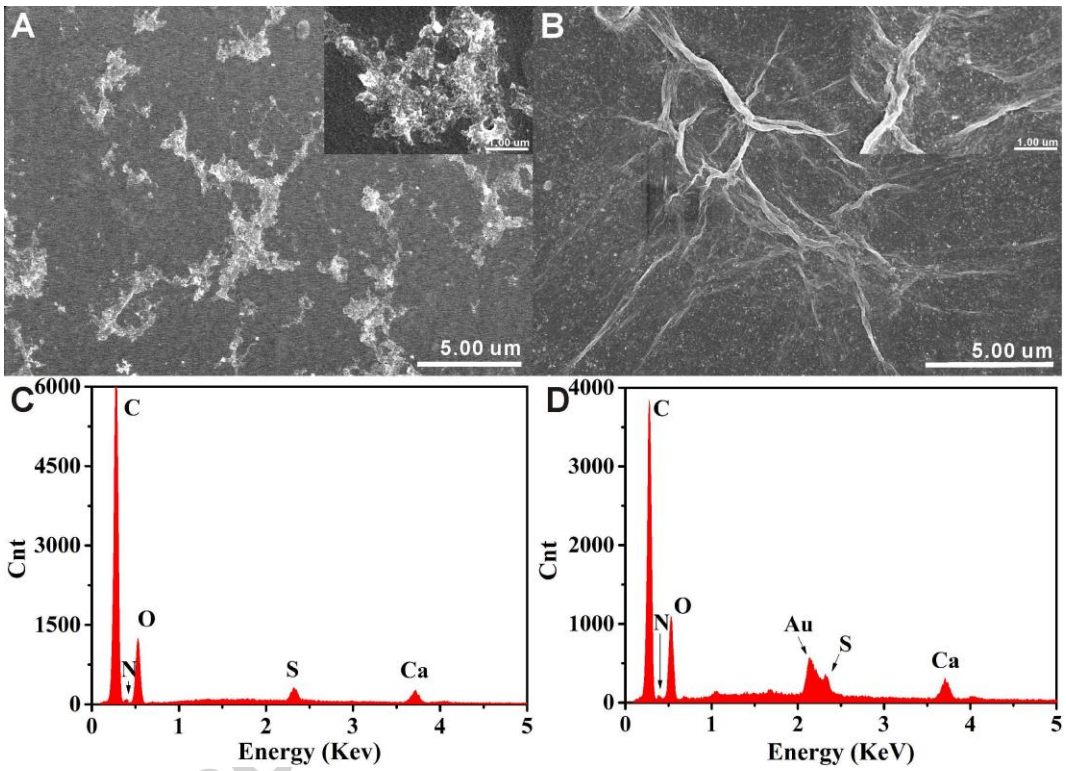
A
5.00 um
B
5.00 um
C
Cnt
C
O
N
S
Ca
Energy (Kev)
D
Cnt
C
O
N
Au
S
Ca
Energy (KeV)

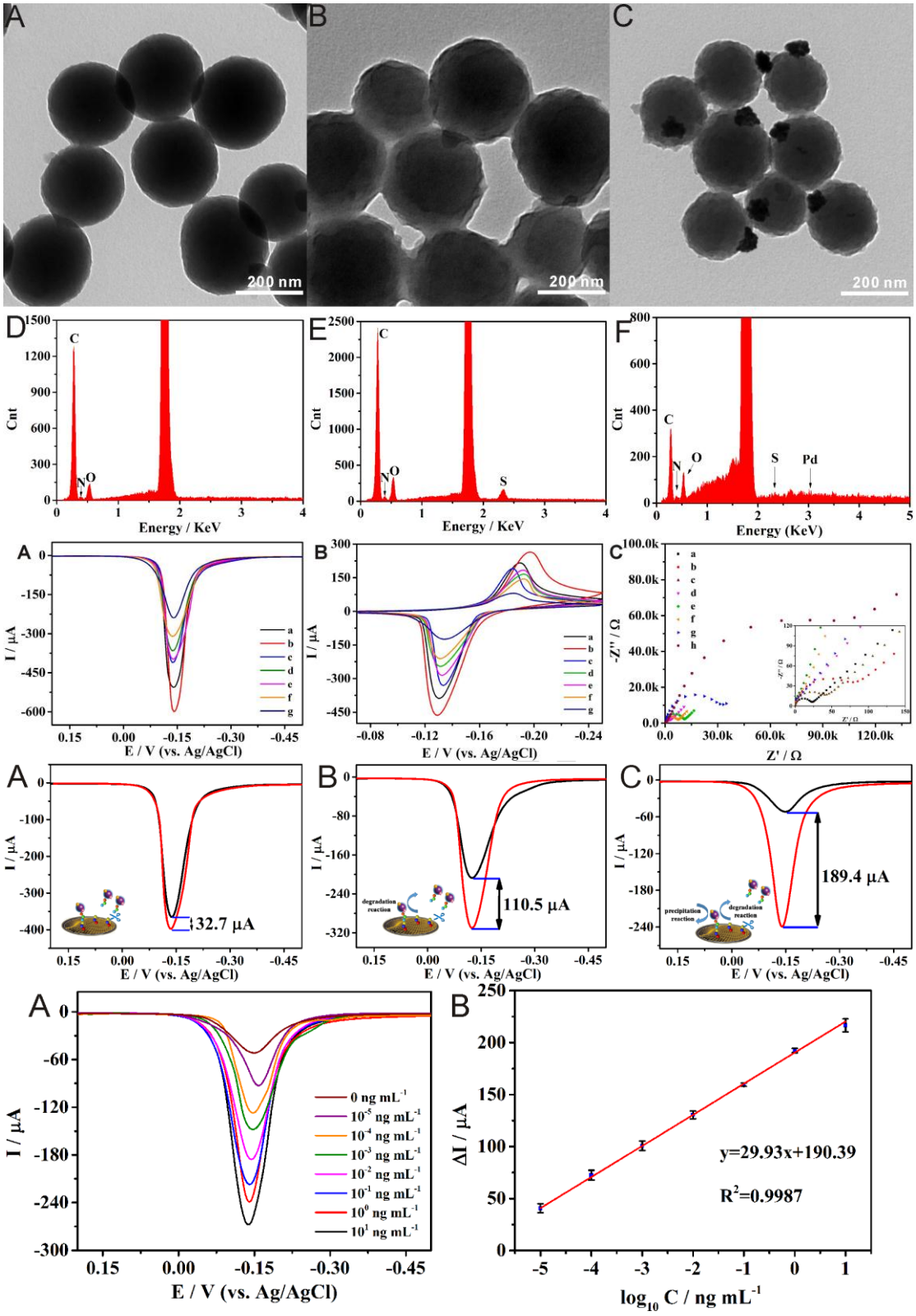
A
B
C
200 nm
200 nm
200 nm
D
E
F
Cnt
Energy / KeV
Energy (KeV)
C
N
O
S
Pd
A
B
C
I / μA
E / V (vs. Ag/AgCl)
-Z'' / Ω
Z' / Ω
32.7 μA
110.5 μA
189.4 μA
degradation reaction
precipitation reaction
0 ng mL-1
10-5 ng mL-1
10-4 ng mL-1
10-3 ng mL-1
10-2 ng mL-1
10-1 ng mL-1
100 ng mL-1
101 ng mL-1
ΔI / μA
y=29.93x+190.39
R2=0.9987
log10 C / ng mL-1